Computational assessment of transport distances in living skeletal muscle fibers studied in situ

Kenth-Arne Hansson[1,2], Andreas Våvang Solbrå[1, 2, 4], Kristian Gundersen[1,2,] and Jo Christiansen Bruusgaard[1,2,3, §]

[1]Department of Biosciences, University of Oslo, Oslo, Norway

[2]Center for Integrative Neuroplasticity, Department of Biosciences, University of Oslo, Oslo Norway

[3]Department of Health Sciences, Kristiania University College, Oslo, Norway

[4]Department of Physics, University of Oslo, Oslo, Norway

[§]Corresponding author

Abstract

Transport distances in skeletal muscle fibers are mitigated by these cells having multiple nuclei. We have studied mouse living slow (soleus) and fast (extensor digitorum longus) muscle fibers in situ and determined cellular dimensions and the positions of all the nuclei within fiber segments. We modelled the effect of placing nuclei optimally and randomly using the nuclei as the origin of a transportation network. It appeared that an equidistant positioning of nuclei minimizes transport distances along the surface for both muscles. In the soleus muscle however, which were richer in nuclei, positioning of nuclei to reduce transport distances to the cytoplasm were of less importance, and these fibers exhibit a pattern not statistically different from a random positioning of nuclei. Together, these results highlight the importance of spatially distribute nuclei to minimize transport distances to the surface when nuclear density is low, while it appears that the distribution are of less importance at higher nuclear densities.

Introduction

The largest cells in the vertebrate body are the muscle fibers, and their vast size introduce logistical problems with respect to synthetic capacity and transport of macromolecules. For example, a human sartorius muscle has an average fiber length of 42 cm (Sandve *et al.*, 2011) and a fiber cross sectional area of about 2500 μm^2 (Kann, 1957) which leads to a volume of 1050 nl. Most other mononucleated cells range 5-20 µm in diameter and, assuming a spherical shape, have volumes less than 0.004 nl. The cell body of an alpha motor neuron might have a diameter of 50 µm and assuming a spherical shape this gives a volume of about 0.07 nl. In addition, it might have an axon spanning 1 m, and with a diameter of 7 µm this yields a volume of 38 nl. The motor neuron might thus be the second largest cell type in a human body, albeit the sartorius cell still has a volume almost 30 times larger. When cells become larger, the average transport distances increase and thus influence the overall transport times. Hence, small and large cells operate under different time scales (Cadart *et al.*, 2019). In larger cells, molecules would acquire longer transport times to reach their target. Because diffusion times, t, scale to the distance travelled L as $t \propto L^2$, diffusion is more efficient at shorter distances. In contrast, active transport times scale linearly to the distance travelled, although the speed relies heavily upon the molecular kinetics of the motor proteins. Typically, a kinesin motor moves at a speed of 1µm/s along the microtubules (Pilling *et al.*, 2006), while the myosin V moves at 3µm/s on the actin filaments (Schott *et al.*, 2002).

47 Mammalian skeletal muscle cells are syncytia, and human muscle cells might
48 have several thousand nuclei (Cristea *et al.*, 2010). The high number density of nuclei
49 is believed to be required due to the large fiber volume and long transport distances,
50 and both the positioning and the nuclear number seems to be regulated to
51 overcome these challenges based on restricted synthetic capacity and the physical
52 limitations to intracellular transport (Bruusgaard *et al.*, 2003; Bruusgaard *et al.*,
53 2006; Metzger *et al.*, 2012b; Gundersen, 2016). We have previously suggested that
54 the myonuclei seems to be distributed as if to repel each other to minimize
55 cytoplasmic transport distances in mammalian fibers (Bruusgaard *et al.*, 2003;
56 Bruusgaard *et al.*, 2006). This optimization seems to be important in the fruit fly as
57 wells (Manhart *et al.*, 2018), since perturbation of the nuclear positioning has been
58 reported to impair muscle function (Metzger *et al.*, 2012a; Folker & Baylies, 2013).

59 The fact that these cells are multinucleated has led to the proposal of a so-
60 called cytoplasmic-to-nucleus domain that signifies a theoretical cytoplasmic domain
61 governed by a single nucleus (Strassburger, 1893). Each nucleus is surrounded by a
62 synthetic machinery that seems to remain localized (Pavlath *et al.*, 1989; Mishra *et*
63 *al.*, 2015), and it has been shown that some proteins are localized in proximity to site
64 of expression both in vitro (Hall & Ralston, 1989; Pavlath *et al.*, 1989; Ralston & Hall,
65 1992a) and in vivo (Merlie & Sanes, 1985; Sanes *et al.*, 1991).

66 In hybrid myotubes in which one or a few nuclei were derived from myoblasts
67 expressing non-muscle proteins it was found that mRNAs for nuclear, cytoplasmic

68 and ER-targeted proteins had similar distributions, and were in most cases confined
69 to distances 25-100 µm from the nuclei (Ralston & Hall, 1992b). Similar observations
70 were made with virus infected isolated muscle fibers in culture, with the additional
71 observation that virus coding mRNA did not venture into the fiber interior but
72 remained around the nucleus at the fiber surface at least for the first 40 hours after
73 infection (Nevalainen *et al.*, 2013). These and other observations support the notion
74 that myonuclei support the expression of different genes within a
75 compartmentalized region of a fiber (Cheek, 1985; Hall & Ralston, 1989; Pavlath *et*
76 *al.*, 1989). The most prominent example is the acetylcholine receptor that is
77 normally expressed only in the nuclei near the endplate, and expression outside this
78 area (acetylcholine super-sensitivity) seems to require that the receptor is
79 transcribed in nuclei along the entire length of the fiber (Merlie *et al.*, 1984;
80 Gundersen & Merlie, 1993).

81 On the other hand, experiments where aggregated blastomeres from two different
82 mouse strains expressing distinct forms of cytosolic metabolic enzymes display
83 heterodimers of the enzyme in the syncytial muscle tissue (Mintz & Baker, 1967),
84 and histological examination displayed no mosaicism in the cellular distribution of
85 the enzyme variants in muscle fibers (Frair & Peterson, 1983). This means that some
86 smaller proteins that are not trapped in structures such as synapses and sarcomeres
87 can be distributed over longer distances, and that the nucleus of origin is of less
88 importance.

To get a better understanding of how nuclear positioning may affect transport distances in muscle fibers we employed precise confocal imaging and 3D reconstruction of fibers labelled in vivo in the soleus and EDL muscle. These muscles differ in their myonuclear density and their nuclear distribution (Bruusgaard *et al.*, 2003), and thus potentially highlight variations in nuclear pattern due to differences in functional needs and composition of the interior. We therefore modelled each nucleus as an origin of transportation network, and derived the area and volume of responsibility by Voronoi segmentation (Du *et al.*, 2010) as well as transport distances to the surface and cytoplasm. Additionally, we used simulations of transport distances to analyze the energy trade-off by letting a protein either diffuse locally from a nucleus or being actively transported.

100 # Results

101 We have analyzed fiber segments of live surface fibers of EDL and soleus muscle in
102 situ. Nuclei were generally confined to the fiber surface, hence we analyzed nuclear
103 domains both in 2D (as surface domains along the sarcolemma) and in 3D (as volume
104 domains of the fiber cytoplasm).

105 **Cross sectional area and nuclear number in individual muscle fibers from the EDL**
106 **and soleus muscle**

107 Quantification of nuclear number after injecting fluorescently labelled
108 oligonucleotides, and fluorescent dextran, revealed that the EDL (Fig. 1A) fibers had
109 approximately half as many nuclei (47±10 nuclei /mm) compared to the soleus fibers
110 (88±29 nuclei/mm) (Fig. 1B). Reconstructions of fiber segments from confocal stacks
111 (Fig. 1C and D) showed that the EDL fibers were about 31% larger than those in the
112 soleus (Fig. 1F). On average, the EDL muscle had a CSA of 1091± 278.4 μm^2 and the
113 soleus 831.8± 241.3 μm^2. These differences in nuclear number and size resulted in
114 EDL fibers having volume domains 130% larger than soleus fibers (Fig. 1G), and 93%
115 larger surface domains than in the soleus (Fig. 1H). The domain volumes in the EDL
116 were on average 23468 ± 5930 μm^3 and 10187 ± 3432 μm^3 in the EDL and soleus
117 muscle, respectively. In the EDL, surface domains were on average 2907 ± 582 μm^2,
118 while in the soleus they were on average 1508 ± 582 μm^2.

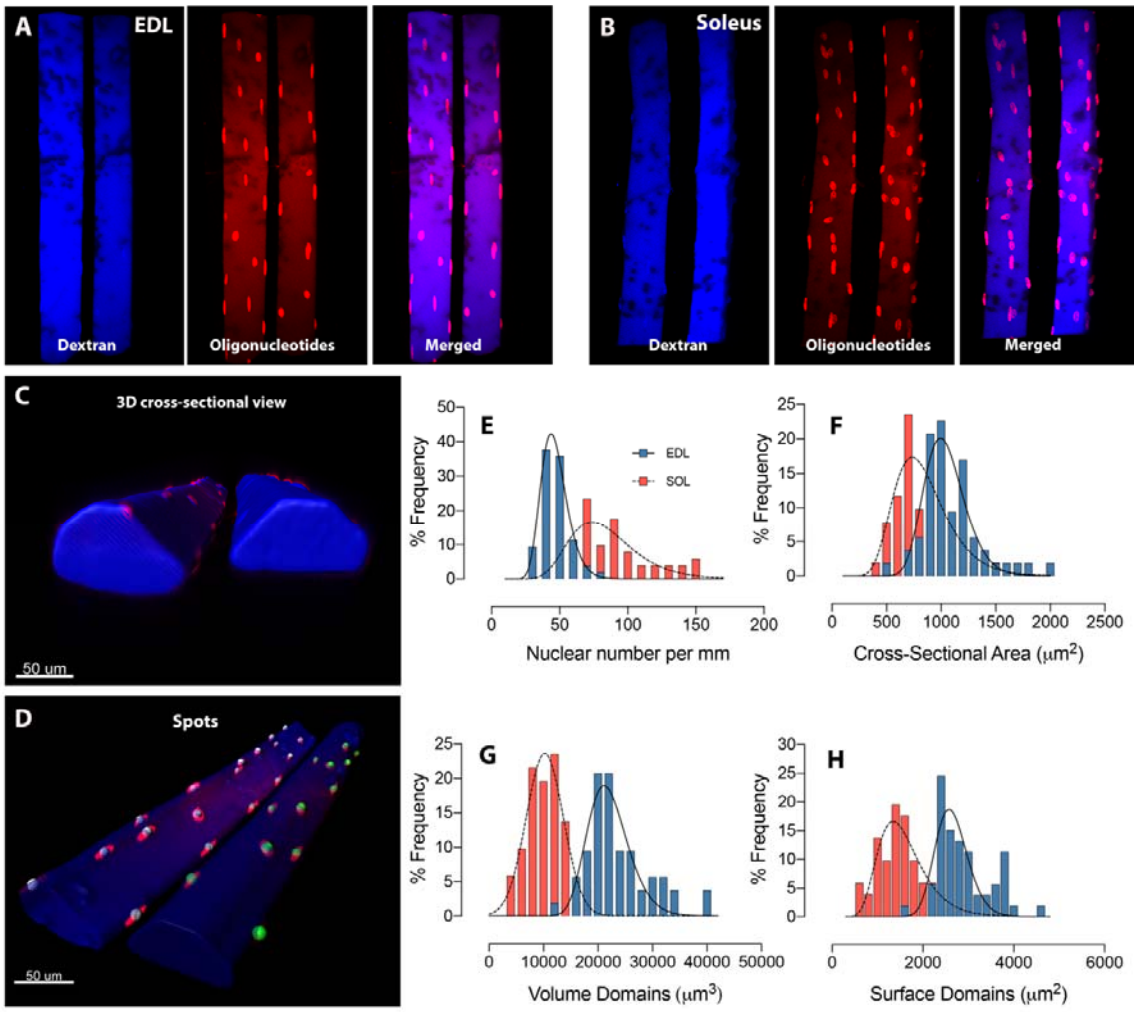

Figure. 1. Three-dimensional modeling of muscle fibers after in vivo injections and confocal imaging. (A) Representative collapsed z-stacks of fibers from the EDL and (B) soleus muscles, injected with dextran (blue) and labelled oligonucleotides (red). (C) 3D modelled fibers based on the fluorescence from the cytosolic dextran. (D) Example of automatic assignment of spots to each myonucleus in order to define their 3D coordinates for subsequent analysis. (E) Frequency distribution of nuclear number and (F) cross sectional area, domain volume (G) and surface domains (H) in the EDL (blue) and soleus muscle (red).

127 **EDL and soleus display pattern differences of their domains**

128 While the average nuclear domains are a simple function of the density of nuclei,
129 and independent of how the nuclei are distributed, our data allowed us to study the
130 distribution of the individual myonuclear domains. In a nuclear distribution where
131 the distance between the nuclei is optimized, all domains would in principle be of
132 equal size. Any deviation from that would imply a non-optimized positioning of
133 nuclei, which may indicate that some domains would be unnecessarily large and
134 represent "lacuna" where transport distances might be rather long.

135 To analyze how individual surface domains is influenced by the distribution of nuclei,
136 we performed a detailed quantification of individual nuclear domains for each
137 nucleus. Voronoi segmentation is a common way of formally quantifying areas or
138 volumes of "influence" for distributed entities of the same kind. We modelled
139 individual Voronoi domains by partitioning the fiber into sub-compartmentalized
140 surface areas and volumes based on the position of each individual nucleus. To
141 compare differences between nuclear distributions in the two muscles we used the
142 standard deviation of the domain sizes. In EDL the observed values for the standard
143 deviation measured for the Voronoi areas were not too different from those
144 obtained when the nuclei were placed optimally, but some fibers showed much
145 larger variability (Fig. 2B), indicating a less optimal distribution with some large
146 lacunar domains. In the soleus, however, the observed pattern resembled more the
147 values obtained when nuclei were placed randomly on the fiber surface (Fig. 2D).

148 There was no obvious difference in the variation of nuclear position with fiber size
149 (Fig. 2C and E).

150 Statistically, domain areas of the observed distribution were different from a
151 random positioning of nuclei (mean difference in the SD of 641μm^2; $p<0.0001$ in the
152 EDL and 194μm^2; $p<0.0001$ in the soleus) as well as optimal positioning (mean
153 difference in the SD of , 405μm^2; $p<0.0001$ for the EDL, and 432μm^2; $p<0.0001$ for
154 the soleus).

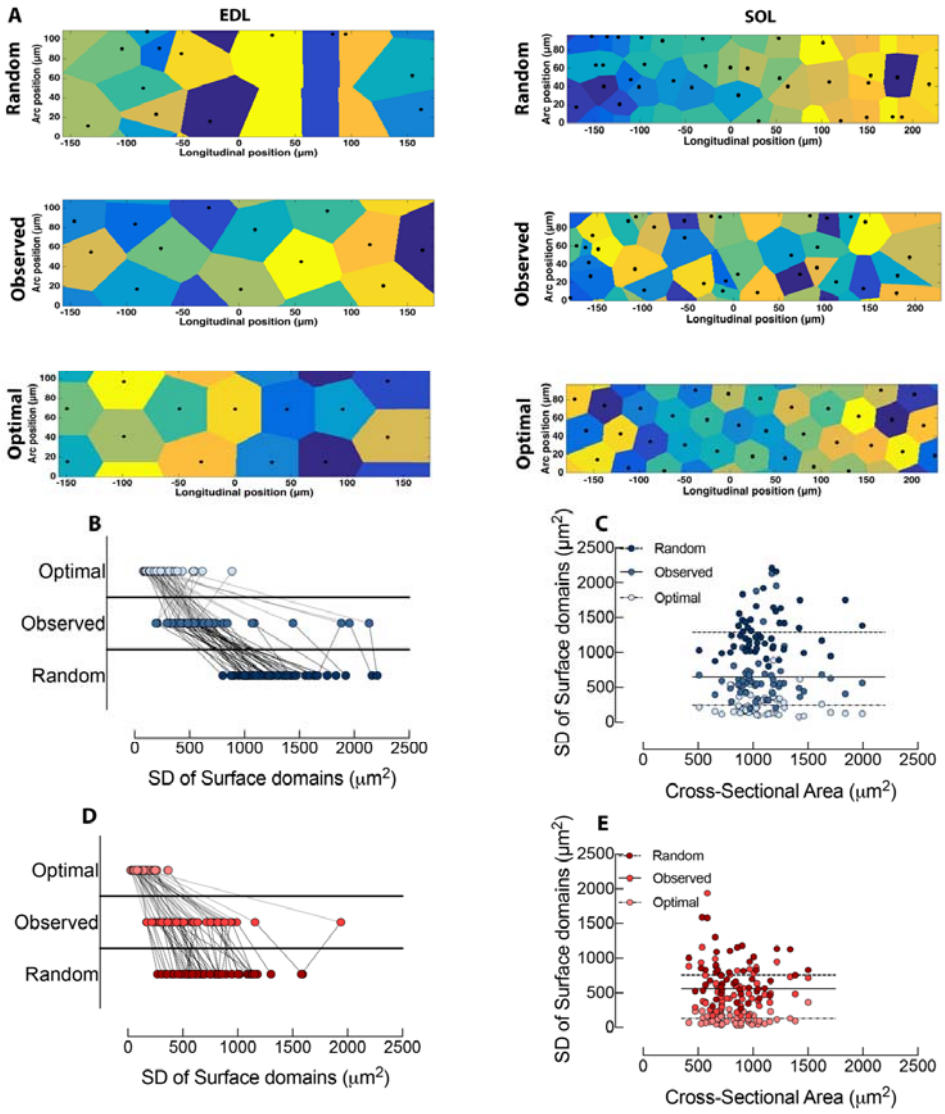

Figure 2. EDL and soleus display differences in patterning of Voronoi areas. (A) Representative Voronoi diagrams of individual domain areas in fibers from the EDL and soleus in the observed distribution and where nuclei were placed randomly or optimally on the fiber surface. (B) Comparison of observed and simulated nuclear patterns in the EDL and (D) soleus muscle plotted as a nested connection between the variation (standard deviation) of individual domains within a single fiber. Dashed and dotted lines signify the inter-specific connection between standardized variation of random-observed and observed-optimal. (C) Variation of surface domains plotted against the cross-sectional area in the EDL and (E) soleus. The relationship between variation and cross-sectional area was non-significant: Random (EDL, p=0.1625; SOL, p=0.5160), observed (EDL, p=0.8844; SOL, p=0.5858) and optimal (EDL, p=0.6892; SOL, p=0.9167).

165 Next, we analyzed the Voronoi volumes (Fig. 3A), the difference between the two
166 muscles resembled the values obtained when comparing Voronoi areas. Thus, in the
167 EDL the variability resembled an optimal distribution (Fig. 3B), whereas in the soleus
168 the variability was closer to placing the nuclei randomly (Fig. 3D). There was no clear
169 effect of fiber size on the variation in Voronoi volumes (Fig. 3C and E).

170 Statistically, domain volumes of the observed distribution were different from a
171 random positioning of nuclei (mean difference, 6521μm^3; $p<0.0001$ in the EDL and
172 mean difference, 224μm^3; $p<0.0001$ in the soleus) as well as optimal positioning
173 (mean difference, 6306μm^3; $p<0.0001$ for the EDL, and 4084μm^3; $p<0.0001$ for the
174 soleus).

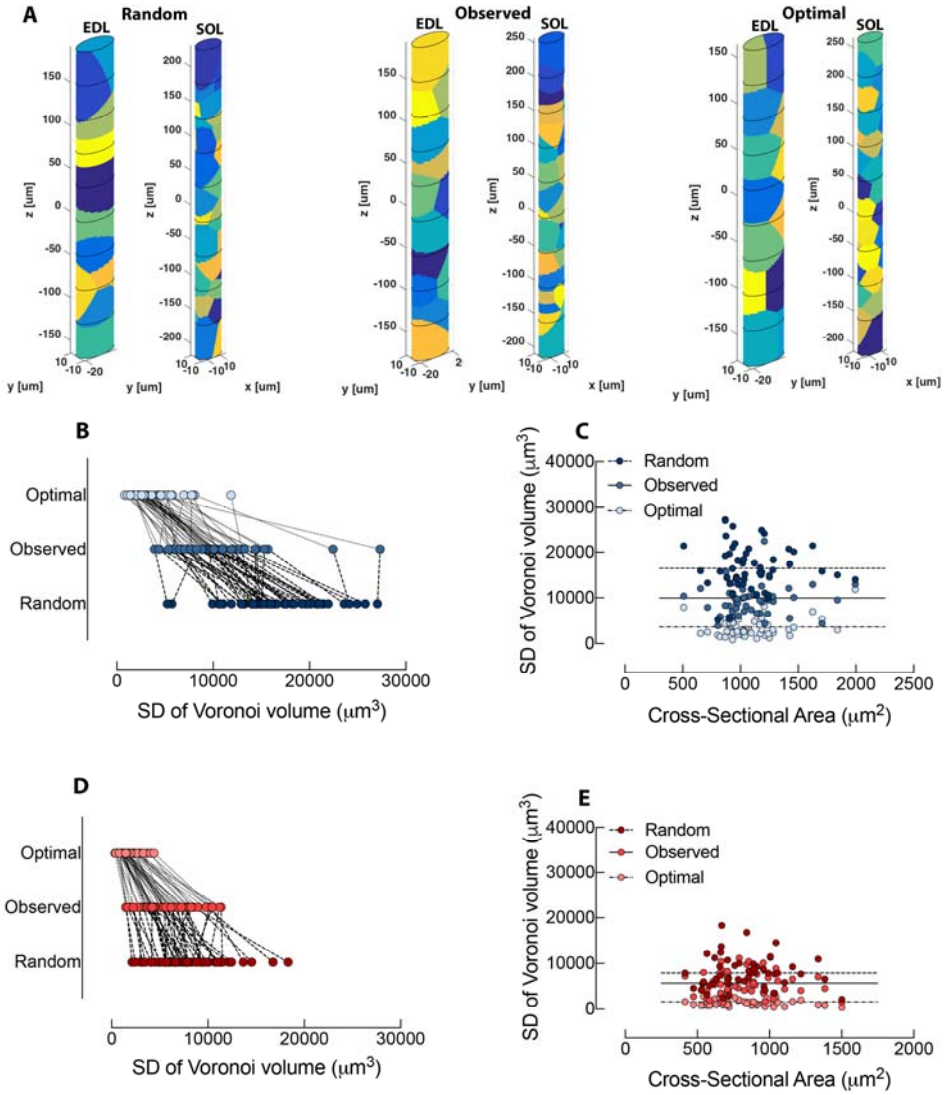

Figure 3. EDL and soleus display differences in patterning of Voronoi volumes. (A) Representative Voronoi diagrams of individual domain volumes in fibers from the EDL and soleus in the observed distribution and where nuclei were placed randomly or optimally on the fiber surface. (B) Comparison of observed and simulated nuclear patterns in the EDL muscle and (D) soleus plotted as a nested connection between the variation (standard deviation) of individual domains within a single fiber. Dashed and dotted lines signify the inter-specific connection between standardized variation of random-observed and observed-optimal. (C) Variation of surface domains plotted against the cross-sectional area in the EDL and (E) soleus. The relationship between variation

183 and cross-sectional area was non-significant: Random (EDL, p=0.9651; SOL, p=0.9965), observed (EDL, p=0.9843;

184 SOL, p=0.8789) and optimal (EDL, p=0.0627; SOL, p=0.4078).

185 **Transport distances vary between the EDL and soleus muscle**

186 The perhaps most relevant measure for judging the importance of nuclear density
187 and positioning is the actual transport distances along the surface or through the
188 cytoplasm. To model this, a grid of points corresponding to the pixel size was placed
189 on the surface or in the volume of each fiber. The closest distance from these points
190 to the nearest nuclei was calculated both on the surface (Fig. 4A) and in the fiber
191 volume (Fig. 5A).

192 Comparing transport distances along the surface between different nuclear
193 distributions showed that on average, EDL fibers had 10% longer transport distances
194 (23± 4.7 µm) compared to the value obtained by placing nuclei optimally (21± 2.5
195 µm). When nuclei were placed randomly (27± 3.2 µm), the average distance were
196 increased by 29% relative to optimal distances and the observed distances were
197 closer to an optimal distribution (Figure 4B). In the soleus muscle, fibers had
198 transport distances (20±9.2 µm) 25% larger compared to the average transport
199 distance when nuclei were placed optimally (16±4.2 µm), while placing nuclei
200 randomly (20±5.5 µm) was essentially identical to the observed distances (Fig. 4C).

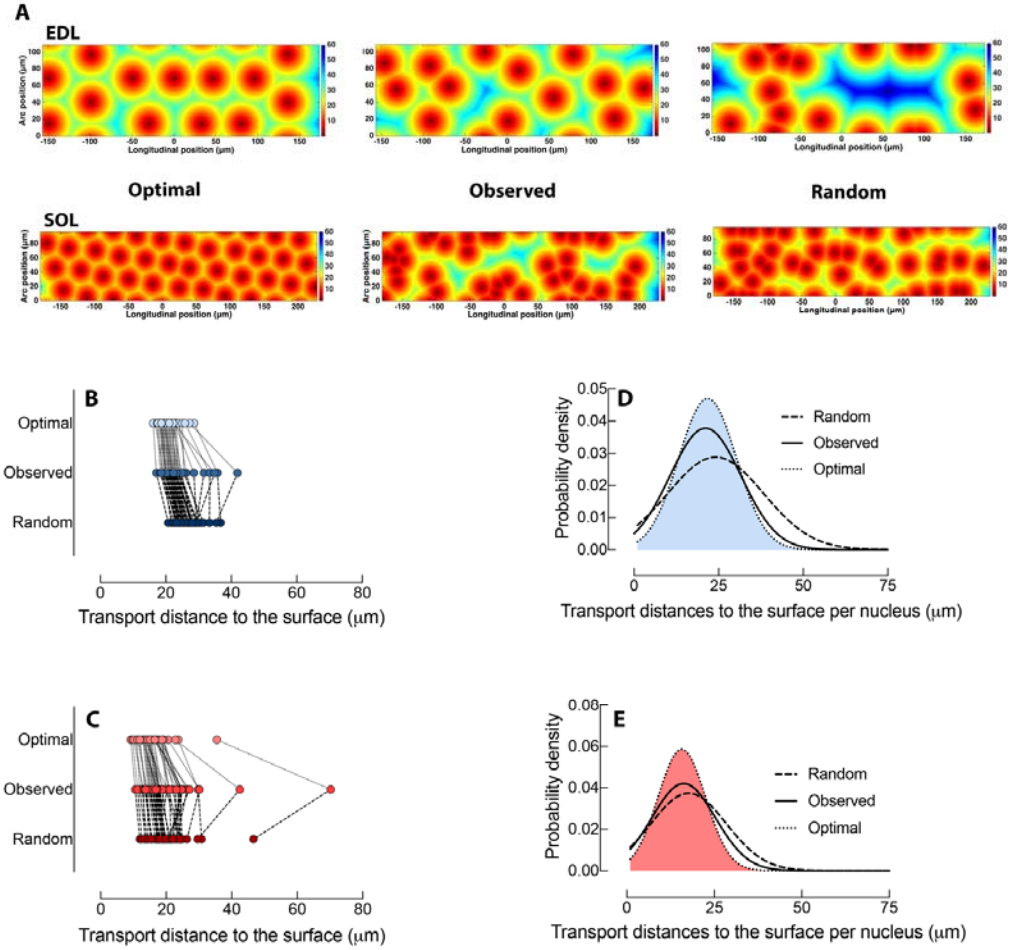

Figure 4. Quantitated measurements of transport distances along the fiber surface. (A) Fiber surface distance maps of fibers in the observed distribution and where nuclei were placed randomly or optimally on the fiber surface. (B-E) The average surface distance to the nearest nucleus were calculated and compared with optimal and random transport distances. (B) Transport distances in the EDL muscle (blue) compared by their mean value per fiber, and per nucleus after a Gaussian fit (D). (C) Transport distances in the soleus muscle (red) compared by their mean value per fiber and per nucleus after a Gaussian fit (E). Dashed and dotted lines in (B and C) signifies the inter-specific connection between random-observed and observed-optimal. The Red-Green-Blue (RGB) vertical scale bar/ color gradient in (A) signifies the distance at 0µm-30µm-60µm from its nuclear origin.

210 For average transport distances in the cytoplasm (Fig. 5B), the observed distances in
211 the EDL (22±3.6 µm) were closer to those seen when nuclei were placed randomly
212 (23±2.7 µm) compared to nuclei placed optimally (21±2.6 µm). Interestingly,
213 distances to the cytoplasm retrieved from placing nuclei randomly (20±5.5 µm) or
214 optimally (17±5.7 µm) in the soleus (Fig. 5C) were not significantly different from
215 observed transport distances (20±7.5µm).

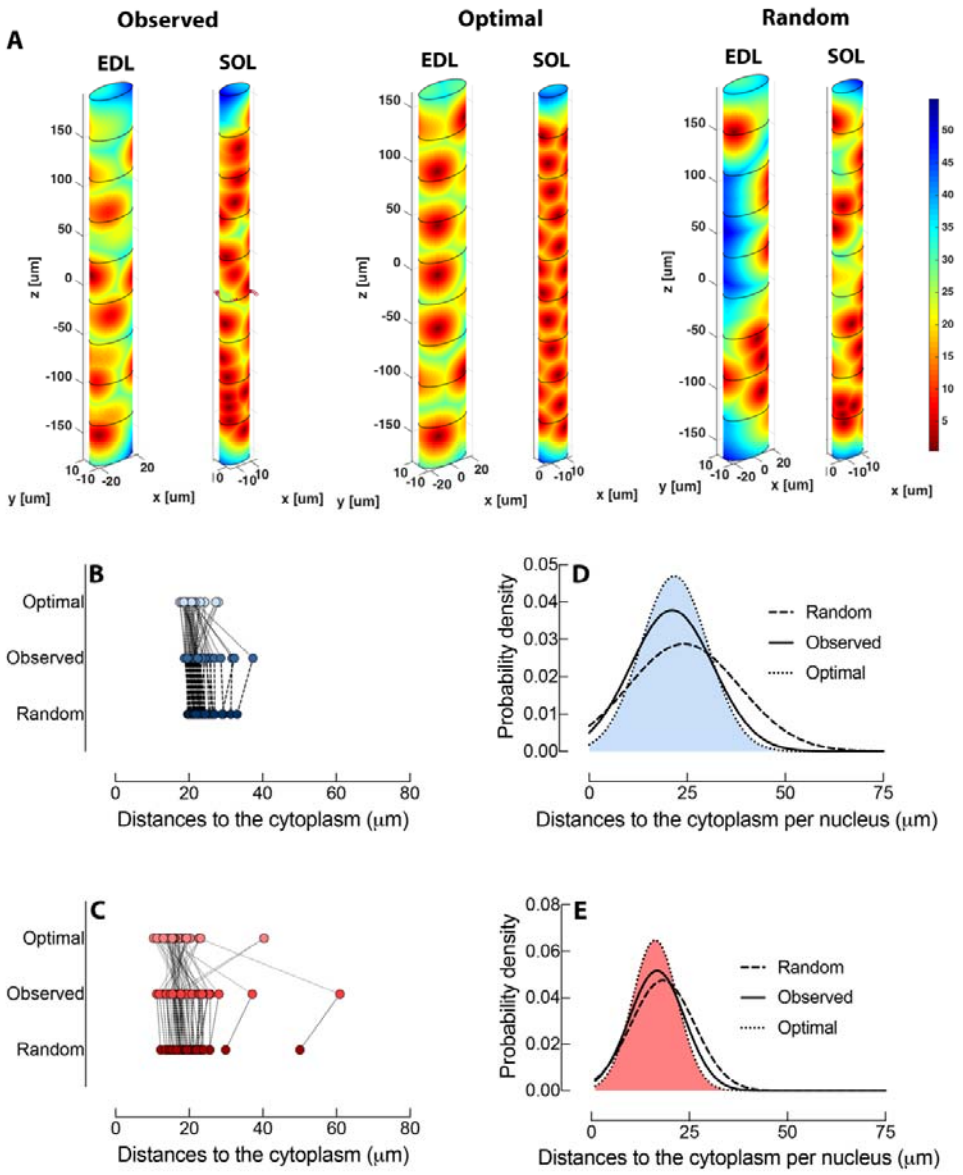

Figure 5. Measurements of transport distances to the cytoplasm. (A) Fiber volume distance maps of fibers where nuclei are placed optimally, randomly, and compared to the observed positioning. (B-E) The average surface distance to the nearest nucleus were calculated and compared with optimal and random transport distances. (B) Transport distances in the EDL muscle (blue) compared by their mean value per fiber and (D), per nucleus after a Gaussian fit. (C) Transport distances in the soleus muscle (red) compared by their mean value per fiber and (E) per nucleus after a Gaussian fit. Dashed and dotted lines in (B and C) signifies the inter-specific

223 connection between random-observed, and observed-optimal. The Red-Green-Blue (RGB) color gradient in (A)
224 signifies the distance at 0μm-30μm -60μm from its nuclear origin.

225

226 In the EDL, there was a statistical improvement in placing nuclei optimally compared
227 to the observed and random transport distances to the surface, and in the cytoplasm
228 (Supp. Fig. 1A, B). However, there was no statistical difference between observed
229 placement of nuclei and their transport distances to the cytoplasm when compared
230 to optimally and randomly positioned nuclei (Supp. Fig.1B). In fibers of the soleus
231 muscle, there was a statistical improvement when placing nuclei optimally for
232 transport distances along the surface (Supp. Fig. 1C), but no improvement within the
233 cytoplasm (Supp. Fig. 1D).

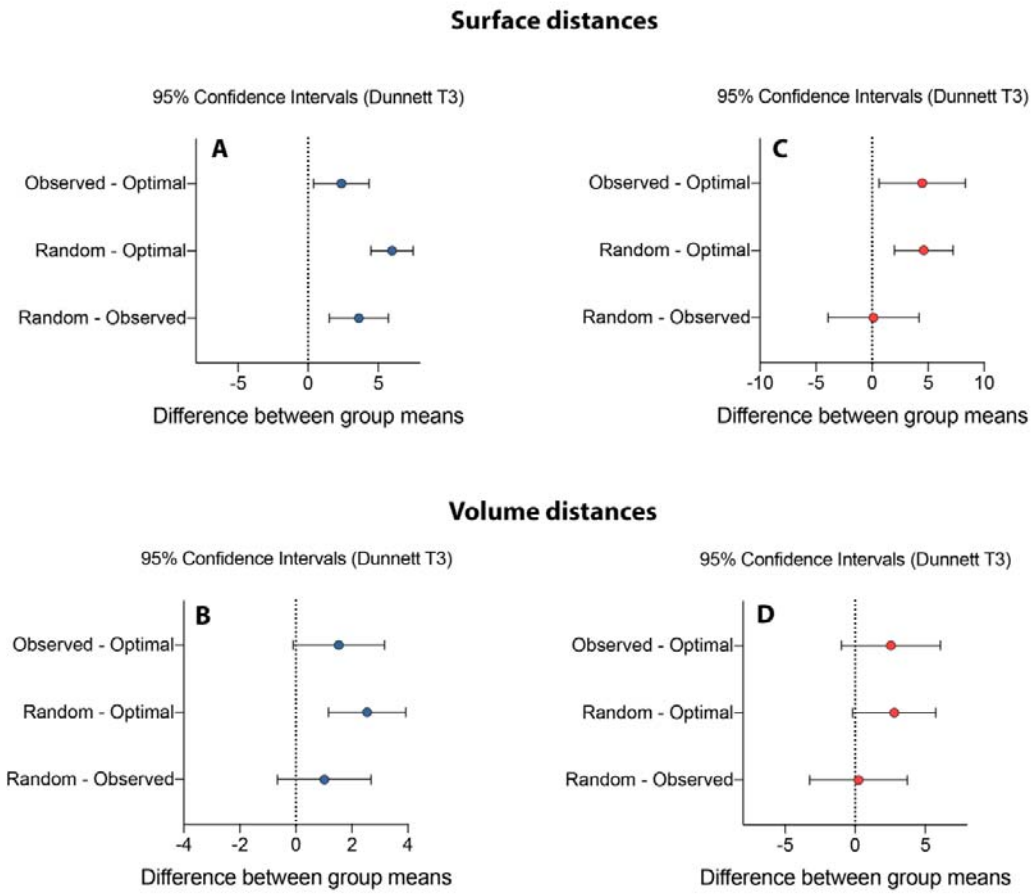

Supplementary figure 1. A group wise Brown-Forsythe analysis of differences in transport distances along the surface (EDL, A; SOL, C) and cytoplasm (EDL, B; SOL, D). For all graphs, 95% confidence intervals overlapping a zero difference between means is regarded as non-significant comparisons. A Dunnett post hoc test were performed to correct for multiple comparisons.

The average transport distance might not reflect whether there are some areas or volumes that is far away from any given nucleus, giving rise to lacunas that might have an insufficient supply of macromolecules. Therefore, we analyzed the distances

243 on a per nucleus basis. Distribution of individual nuclear distances were fitted with a
244 Gaussian function (Fig. 4D, E and Fig. 5D, E). It was evident from the Gaussian fit that
245 the actual transport distances along the surface in the EDL where much improved
246 compared to a random distribution and was approximating an optimal distribution
247 (Fig. 4D). Similar conclusions were obtained analyzing optimal transport distances in
248 the cytoplasm (Fig. 5D). Notably the longer transport distances were less prevalent
249 by the observed placement of nuclei compared to a random distribution.

250 Soleus displayed similar traits when the transport distances along the surface (Fig.
251 4E) and cytoplasm (Fig. 5E) was analyzed, but the observed distribution was more
252 similar to a random distribution.

253 In the EDL we found that 37% of the surface was longer than 25µm from the nearest
254 nucleus, compared to 28% when nuclei were placed optimally and 47% randomly. In
255 the soleus 27% of the fiber surface were longer than 25 µm from the nearest nucleus
256 in the observed distribution, compared to 8% and 23% in the optimal and random
257 distribution, respectively. Interestingly, and despite differences in fiber size and
258 nuclear number, both muscles displayed about 97% of their surface to be within 50
259 µm of its nearest nucleus (Table I)

260

261

262

TABLE I. Percent of the cytosol or surface to its nearest nucleus at different distances

	Distance (µm)	Observed (%)		Optimal (%)		Random (%)	
		EDL	Soleus	EDL	Soleus	EDL	Soleus
Surface	0-25	63	77	72	92	53	73
	25-50	34	20	28	7	41	25
	> 50	3	3	0	1	6	2
Cytosol	0-25	69	79	77	88	62	77
	25-50	30	18	23	11	36	22
	> 50	1	3	1	1	2	1

In terms of volumes, 31% of the cytoplasm in the EDL were longer then 25 µm from its nearest nucleus during observed distributions, increasing to 38 % when nuclei were placed randomly, and 23% with optimal distribution of the nuclei. The soleus muscle displayed overall shorter transport distances as only 21% of the cytoplasm was more than 25 µm from its nearest nucleus, increasing only slightly to 23% when nuclei were randomly distributed, and 12% optimally. In spite of differences between the two muscles with respect to distances within 25 µm, 98% of the cytoplasm resides within a 50 µm proximity to the nearest nucleus.

273 **Consequences for diffusion times**

274 We here describe the differences in dimensions, distribution and density of
275 myonuclei in fibers from solus and EDL. It has however, previously been reported
276 that also the effective diffusion coefficient differs in fibers from these two muscles
277 (Papadopoulos *et al.*, 2000), and measured to be 12.5×10^{-8} cm^2s^{-1} and 18.7×10^{-8}
278 cm^2s^{-1} in soleus and EDL respectively. When combined with our data, this
279 information allows us to calculate diffusion times (t) from the nearest nuclei to any
280 point in the cell according to $t = L^2/2\sigma D$, where L is the transport distance in σ
281 dimensions, and D is the effective diffusion coefficient. The average diffusion times
282 are given for each fiber in Fig. 6 and is compared to transport times that would be
283 obtained by active transport (see Introduction).

284 We used myoglobin as an example and calculated the transportation times to each
285 point on the surface. On average, we calculated transport times to be 8.2± 1.5s and
286 8.4± 1.8s for EDL and soleus respectively (Fig. 6A). For the diffusion times to each
287 point in the entire cytoplasmic volume, the geometric mean was 5.0± 1.3s and 5.4±
288 1.6s for EDL and soleus respectively (Fig.6B). Thus, in spite of the large differences in
289 dimensions, nuclear density and nuclear distribution, the diffusion time was
290 remarkably similar for the two muscles.

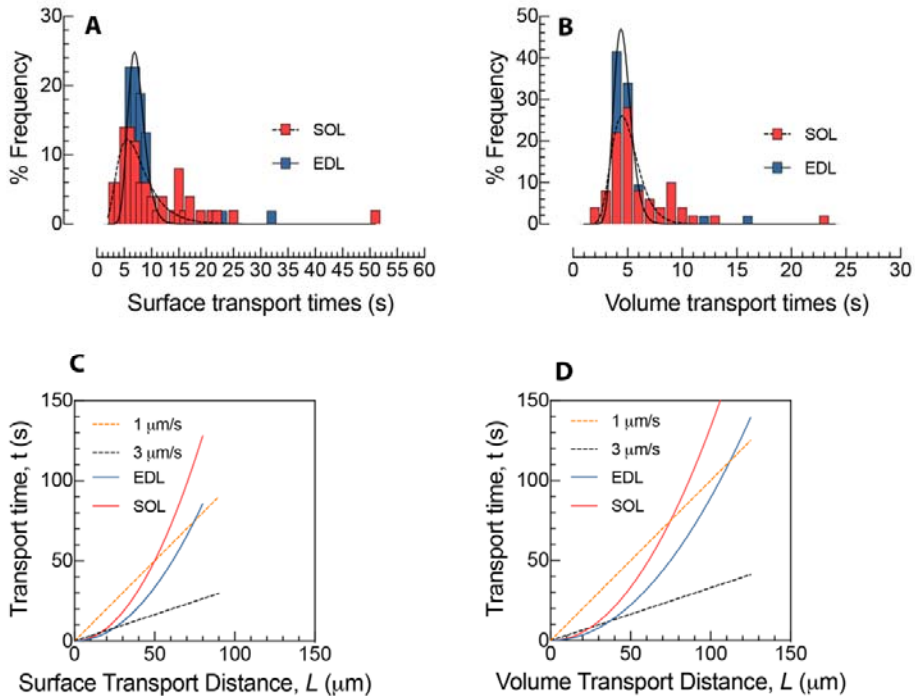

Figure 6. EDL and soleus muscle display roughly equal diffusion times. (A) Diffusion times plotted as the relative frequency distribution versus time along the surface and (B) within the fiber volume. (C) Transport times against distances along the surface and (D) within the volume Active transport at a speed of 3μm/s are highlighted by dashed lines. The intersection between dashed lines and the curvilinear data points highlight the interface where diffusion and active transport have equal transport times. At transport distances larger than the intersection, active transport is faster than diffusion.

It is likely that intracellular transport in muscle relies both on active and passive transport. Active transport along microtubules has been described in skeletal muscle (Pizon *et al.*, 2005; Wang *et al.*, 2013). While we are not aware of data on myosin mediated transport along actin in skeletal muscle, myosin IV has been observed localized to the fiber periphery, nuclei, sarcoplasmic reticulum and at the neuromuscular junction (Karolczak *et al.*, 2013), and the thick-filament-associated

304 myosin molecule seems to be replaced in cultured myotubes in the absence of the
305 microtubule system (Ojima *et al.*, 2015), while the actin network *per se* seems to be
306 imperative for transport of membrane located molecules like e.g. the insulin
307 sensitive glucose translocator GLUT4 (Brozinick *et al.*, 2004).

308 For the transport along the surface, diffusion would be faster than actin mediated
309 transport (3μm/s) for distances of less than 15 μm in the soleus and 25 μm in the
310 EDL. When compared to transport along microtubule, diffusion would be faster for
311 distances up to 50 μm in the soleus and 75 μm in the EDL. (Fig. 6C).

312 When allowed to diffuse in three dimensions (Fig. 6D), diffusion would be faster than
313 actin mediated transport for distances of less than 24 μm in the soleus and 36 μm in
314 the EDL. When compared to transport along microtubule, diffusion would be faster
315 for distances up to 75 μm in the soleus and 112 μm in the EDL.

316

317 ## Discussion

318 We here present precise data for cell dimensions, and myonuclear density and
319 positioning in fiber segments of living muscle fibers from EDL and soleus in situ.
320 Fibers from these muscles varied with respect to all these variables, thus the radial
321 size of the EDL fibers was 31% larger than those in the soleus, while the surface or
322 volume per nuclei was 93% and 130% larger than in the soleus, respectively. In spite
323 of these differences, the transport times to points on the surface or in the cytosol
324 are remarkably similar in soleus and EDL, and we hypothesize that fibers are
325 adapting the number and positioning of nuclei in order to achieve certain transport
326 times for relevant macromolecules to all parts of the cell.

327 Given the differences in the variables related to cell dimensions and myonuclei it
328 might seem like a paradox that the diffusion times are so similar, but is explained
329 firstly by the diffusion coefficient being 50% higher in the EDL than in the soleus,
330 secondly, we show that the nuclei are placed more optimally in the EDL. If the nuclei
331 in the EDL were placed randomly, the average surface transport distance (~27μm)
332 versus the distance observed (~23μm) would yield about 40% longer diffusion times,
333 this would translate into a 30% lower concentration of a macromolecule at any given
334 point, and the non-random positioning thus seems to be important in the EDL, and
335 cytoplasmic dilution has been associated with impaired cell function in proliferative
336 cells (Miettinen & Bjorklund, 2016; Neurohr *et al.*, 2019).

337 In contrast, in the soleus the placement of nuclei appeared close to random. It is
338 possible that optimalisation of positioning is less critical since the density of nuclei is
339 higher, another explanation is that other needs override those related to internal cell
340 transport in oxidative muscles, thus in the rat soleus 81% of the nuclei appear next
341 to blood vessels (Ralston *et al.*, 2006).

342 The interior of any cell is greatly crowded by macromolecules such as ribosomes,
343 RNA and proteins (Zhou *et al.*, 2008; Smith *et al.*, 2017), which effectively reduce the
344 motion of molecules and thereby impede diffusion. Additionally, muscle fibers have
345 a dense mesh of myofibrils that occupy 80% of their total volume (van Ekeren *et al.*,
346 1992), which seems to act as exclusion zones for larger macromolecules
347 (Papadopoulos *et al.*, 2000). Taking into account the effects of macromolecular
348 crowding and scaling of transport times, it has been argued that mononuclear cells
349 have small sizes in order to optimize diffusion and signaling (Soh *et al.*, 2013). They
350 found the optimal size of a eukaryotic cell to have a radius of about 10 μm, about
351 half of the transport distance found for muscle fibers in our calculations. This
352 problem might be aggravated, since all nuclei do not express all genes at a given
353 time-point (Fontaine & Changeux, 1989; Newlands *et al.*, 1998). Thus, the transport
354 distances reported here might represent a bottleneck limiting cell function and size
355 of muscle fibers.

356 Disturbance of myonuclear placement impairs muscle function e.g. after mutations
357 in the Drosophila larvae (Metzger *et al.*, 2012b; Folker & Baylies, 2013). In mammals

358 denervation, which leads to grave atrophy and is accompanied by myonuclear
359 clustering eventually leaving lacunas with long transport distances (see introduction)
360 (Viguie *et al.*, 1997; Ralston *et al.*, 1999). Similarly, nuclear distribution is disturbed in
361 several myopathies and might play a causative role in impairing function (Romero,
362 2010).

363 # Material and Methods

364 ## Animals

365 A total of 23 female NMRI mice of 20-30 grams of weight were used. The animal
366 experiments were approved by the Norwegian Animal Research Authority and were
367 conducted in accordance with the Norwegian Animal Welfare Act of 20th December
368 1974. The Norwegian Animal Research Authority provided governance to ensure
369 that facilities and experiments were in accordance with the Act, National Regulations
370 of January 15th 1996, and the European Convention for the Protection of Vertebrate
371 Animals Used for Experimental and Other Scientific Purposes of March 18th, 1986.

372 ## Preparing the mice for imaging

373 Before surgery, animals were anesthetized by a single intraperitoneal injection of a
374 zrf cocktail (18.7 mg zolazepam, 18.7 mg tiletamine, 0.45 mg xylazine and 2.6 mg
375 fentanyl per ml) that were administered at a dose of 0.08 ml per 20 g body weight.

376 The skin over the tibialis anterior and gastrocnemius was shaved and a small incision
377 was made to expose the overlaying muscles that were subsequently retracted
378 laterally to expose the EDL and soleus muscle, respectively. The epimysium was
379 gently removed, and we took care not to damage the muscle. The exposed muscle
380 was covered with a mouse Ringer's solution; NaCl 154mM, KCl 5.6 mM, $MgCl_2$ 2.2
381 mM and $NaHCO_3$ 2.4 mM, and held in place with a coverslip mounted approximately
382 2 mm above the muscle. In some muscles, the neuromuscular end plate was

383 visualized by applying Alexa 488-conjugated α-bungarotoxin (Molecular probes) to
384 the surface of the muscle for 2–3 min.

385 In vivo intracellular injections of intravital dyes were essentially done as described
386 previously (Utvik *et al.*, 1999). Animals were placed under a fixed-stage fluorescence
387 microscope (Olympus BX50WI, Olympus, Japan) with a 20X, NA 0.3, long working
388 distance water immersion objective. For *in vivo* labelling of nuclei and cytoplasm,
389 single fibers in the EDL and soleus were injected with a solution containing 5′ -
390 TRITC or FITC-labelled random 17-mer oligonucleotide with a phosphorothioated
391 backbone (Yorkshire Biosciences Ltd, Heslington, United Kingdom) and 2mg/ml
392 Cascade blue dextran (10kDa, Molecular probes) dissolved in an injection buffer (10
393 mm NaCl, 10 mm Tris, pH 7.5, 0.1 mM EDTA and 100 mM potassium gluconate) at a
394 final concentration of 0.5mM and 1mM, respectively. The oligonucleotides are taken
395 up into the nuclei inside the injected fibers probably by an active transport
396 mechanism (Hartig *et al.*, 1998), while dextran remain in the cytoplasm.

397 **Confocal Imaging**

398 Muscle fibers and nuclei in the EDL and soleus were imaged with a confocal
399 microscope (Olympus FluoView 1000, BX61W1, Olympus, Japan) in optical sections,
400 separated by z-axis steps of 1 µm to have the full three-dimensional data set of
401 nuclei. Sequential scanned fields of 0,09 mm^2 were captured, with a pixel dwell time
402 of 2µs. Movements induced by the mouse heartbeat or ventilation sometimes
403 caused displacements of individual nuclei within stacks. Therefore, mice were given

404 an overdose of the anaesthetics and image acquisition continued for 20 minutes
405 after euthanasia. No difference in myonuclear positioning and fiber morphology was
406 observed before and after euthanasia.

407 **Image analyzis**

408 In vivo images (320 x 640 pixels x 2 µm voxel depth) from optical sections of muscle
409 fibers were imported and analyzed for myonuclear number, 3D myonuclear
410 positioning, fiber volume and surface area using the Imaris bitplane 8.3.1 software
411 (Bitplane). Using the spot function in Imaris, a spot was automatically assigned to
412 each nucleus based on the fluorescence intensity from the injected oligonucleotides,
413 and if misaligned, spots were manually re-positioned to the center of each
414 myonucleus. Highlighted spots/nuclei within fibers were then given a 3D coordinate
415 in a relative Euclidean space using the Imaris Vantage extension. Volume and surface
416 rendering were performed using the fluorescence from Cascade blue conjugated
417 dextran in the cytoplasm. Rendering of fiber volume was performed using the
418 fluorescence perimeter border of the fiber in the cross-sectional direction as an
419 outer limit, and thereby preserving fiber morphology during quantification.

420 **Computer modelling of nuclear distribution**

421 Once the Euclidian coordinates of the myonuclei were obtained in Imaris, fiber
422 surfaces were approximated by fitting the points to the surface of an idealized
423 elliptical cylinder surface.

An elliptical cylinder oriented along the *z*-axis, with its major and minor axes oriented along the *x*- and *y*-axes, respectively, can be parameterized as

$$\frac{(x-x_0)^2}{a^2} + \frac{(y-y_0)^2}{b^2} = 1,$$

where a and b are the major and minor axes, respectively, and is the point where the center of the cylinder intercepts the *xy*-plane.

The cylinder was parameterized by the Euler angles pointing along the z-axis of the cylinder, the major and minor axes of the ellipse, the angle of the major axis relative to the x-axis, and the x- and y-coordinates of the center of the ellipse, for a total of 8 free variables. The optimization was carried out in two rounds, where the Euler angles were chosen first, after which the remaining ellipse fitting was completed for the given angles, using a direct least squares fitting. The angles were then updated using MATLABs interior point optimization solver, until convergence was achieved.

Subsequently, the 3-dimensional coordinates of the nuclei retrieved form Imaris were mapped to the 2-dimensional coordinates consisting of the position along the z-axis and distance along the ellipse circumference relative to the major axis. Next, we calculated area and volumes defined by Voronoi geometries of each nucleus and distance maps for all points on the cylinder surface to the nearest nuclei, based on the distance along the cylinder surface, noting that the surface is periodic along the circumference.

444 Additionally, we ran Monte Carlo simulations and nuclei were randomly placed on
445 the parameterized surface in order to compare the distance map to that of the
446 observed fibers. By a Lloyd's Algorithm, we also placed the nuclei optimally on the
447 surface, such that the Voronoi domains for all nuclei were equal and compared it to
448 an observed distribution of nuclear patterns.

449 All codes used in the computational modelling can be found at
450 https://github.com/CINPLA/cylinderTools.

451 **Statistics**

452 Data were derived from 53 fibers injected on the lateral surface of EDL (N=9 animals)
453 and 51 fibers injected at dorsal surface of the soleus muscle (N=12 animals).
454 Descriptive statistics are shown as the pooled sum of fibers for a given muscle. If not
455 stated otherwise, numbers are presented as mean± standard deviation (mean± SD).
456 Frequently, point pattern analysis, including Voronoi segmentation, subdivide the
457 area or volume of interest into a subset of polygons (2D) or polyhedrons (3D). In
458 Voronoi segmentation, the number of Voronoi polygons is proportional to number of
459 points in the plane or room. In our case, the number of points is equal to the nuclear
460 number within each muscle fiber. Thus, if an area (or volume) is divided into the
461 same number of domain objects, the average size of objects remains the same in
462 spite of differences in the nuclear patterning (i.e. because the total area, volume and
463 number of points are unchanged). Instead, we used the variation (standard
464 deviation) as a measure of similarity between the observed mean size of polygons,

465 to those when nuclei were placed randomly or optimally. We statistically compared
466 standard deviations of domain areas and domain volumes by differences in nuclear
467 patterning by a one-way ANOVA followed by a Tukey's correction for multiple
468 comparisons.

469 In comparison, we are not faced with the same problem as outlined for the Voronoi
470 segmentation when analyzing transport distances between different nuclear
471 distributions. They were therefore analyzed statistically by a Brown-Forsythe analysis
472 followed by a Games-Howell's multiple comparisons test at a 5 % significance level.

473 All graphs and statistical analyzis were plotted and performed in Prism 8 (Graphpad).
474

475 **References**

476 Brozinick JT, Jr., Hawkins ED, Strawbridge AB & Elmendorf JS. (2004). Disruption
477 of cortical actin in skeletal muscle demonstrates an essential role of the
478 cytoskeleton in glucose transporter 4 translocation in insulin-sensitive
479 tissues. *J Biol Chem* **279,** 40699-40706.

480

481 Bruusgaard JC, Liestol K, Ekmark M, Kollstad K & Gundersen K. (2003). Number
482 and spatial distribution of nuclei in the muscle fibres of normal mice
483 studied in vivo. *J Physiol* **551,** 467-478.

484

485 Bruusgaard JC, Liestol K & Gundersen K. (2006). Distribution of myonuclei and
486 microtubules in live muscle fibers of young, middle-aged, and old mice. *J*
487 *Appl Physiol (1985)* **100,** 2024-2030.

488

489 Cadart C, Venkova L, Recho P, Lagomarsino MC & Piel M. (2019). The physics of
490 cell-size regulation across timescales. *Nat Phys* **15,** 993-1004.

491

492 Cheek DB. (1985). The control of cell mass and replication. The DNA unit--a
493 personal 20-year study. *Early Hum Dev* **12,** 211-239.

494

495 Cristea A, Qaisar R, Edlund PK, Lindblad J, Bengtsson E & Larsson L. (2010).
496 Effects of aging and gender on the spatial organization of nuclei in single
497 human skeletal muscle cells. *Aging Cell* **9,** 685-697.

498

499 Du Q, Gunzburger M & Ju LL. (2010). Advances in Studies and Applications of
500 Centroidal Voronoi Tessellations. *Numer Math-Theory Me* **3,** 119-142.

501

502 Folker ES & Baylies MK. (2013). Nuclear positioning in muscle development and
503 disease. *Front Physiol* **4,** 363.

504

505 Fontaine B & Changeux JP. (1989). Localization of nicotinic acetylcholine
506 receptor a-subunit transcripts during myogenesis and motor endplate
507 development in the chick. *J Cell Biol* **108,** 1025-1037.

508

509 Frair PM & Peterson AC. (1983). The nuclear-cytoplasmic relationship in 'mosaic'
510 skeletal muscle fibers from mouse chimaeras. *Exp Cell Res* **145,** 167-178.

511

512 Gundersen K. (2016). Muscle memory and a new cellular model for muscle
513 atrophy and hypertrophy. *J Exp Biol* **219,** 235-242.

514

515 Gundersen K & Merlie JP. (1993). Regulation of nicotinic acetyl choline receptor
516 genes by overexpressing myogenin and Id in transgenic mice. *Society for*
517 *Neuroscience Abstracts* **19,** 223.

518

519 Hall ZW & Ralston E. (1989). Nuclear domains in muscle cells. *Cell* **59,** 771-772.

520

521 Hartig R, Shoeman RL, Janetzko A, Grüb S & Traub P. (1998). Active nuclear
522 import of singel-stranded oligonucleotides and their complexes with non-
523 karyophilic macromolcules. *Biology og the Cell* **90,** 407-426.

524

525 Kann F. (1957). [Diameter and number of muscle fibers in various cross section
526 levels of sartorius muscle in man]. *Acta Anat (Basel)* **30,** 351-357.

527

528 Karolczak J, Sobczak M, Majewski L, Yeghiazaryan M, Jakubiec-Puka A, Ehler E,
529 Slawinska U, Wilczynski GM & Redowicz MJ. (2013). Myosin VI in skeletal
530 muscle: its localization in the sarcoplasmic reticulum, neuromuscular
531 junction and muscle nuclei. *Histochem Cell Biol* **139,** 873-885.

532

533 Manhart A, Windner S, Baylies M & Mogilner A. (2018). Mechanical positioning of
534 multiple nuclei in muscle cells. *PLoS Comput Biol* **14,** e1006208.

535

536 Merlie JP, Isenberg KE, Russell SD & Sanes JR. (1984). Denervation
537 supersensitivity in skeletal muscle: analysis with a cloned cDNA probe. *J*
538 *Cell Biol* **99,** 332-335.

539

540 Merlie JP & Sanes JR. (1985). Concentration of acetylcholine receptor mRNA in
541 synaptic regions of adult muscle fibres. *Nature* **317,** 66-68.

542

543 Metzger T, Gache V, Xu M, Cadot B, Folker E, Richardson BE, Gomes ER & Baylies
544 MK. (2012a). MAP and kinesin-dependent nuclear positioning is required
545 for skeletal muscle function. *Nature* **484,** 120.

546

547 Metzger T, Gache V, Xu M, Cadot B, Folker ES, Richardson BE, Gomes ER & Baylies
548 MK. (2012b). MAP and kinesin-dependent nuclear positioning is required
549 for skeletal muscle function. *Nature* **484,** 120-124.

550

551 Miettinen TP & Bjorklund M. (2016). Cellular Allometry of Mitochondrial
552 Functionality Establishes the Optimal Cell Size. *Dev Cell* **39,** 370-382.

553

554 Mintz B & Baker WW. (1967). Normal mammalian muscle differentiation and
555 gene control of isocitrate dehydrogenase synthesis. *Proc Natl Acad Sci U S*
556 *A* **58,** 592-598.

557

558 Mishra P, Varuzhanyan G, Pham AH & Chan DC. (2015). Mitochondrial Dynamics
559 is a Distinguishing Feature of Skeletal Muscle Fiber Types and Regulates
560 Organellar Compartmentalization. *Cell Metab* **22,** 1033-1044.

561

562 Neurohr GE, Terry RL, Lengefeld J, Bonney M, Brittingham GP, Moretto F,
563 Miettinen TP, Vaites LP, Soares LM, Paulo JA, Harper JW, Buratowski S,
564 Manalis S, van Werven FJ, Holt LJ & Amon A. (2019). Excessive Cell
565 Growth Causes Cytoplasm Dilution And Contributes to Senescence. *Cell*
566 **176,** 1083-1097 e1018.

567

568 Nevalainen M, Kaakinen M & Metsikko K. (2013). Distribution of mRNA
569 transcripts and translation activity in skeletal myofibers. *Cell Tissue Res*
570 **353,** 539-548.

571

572 Newlands S, Levitt LK, Robinson CS, Karpf AB, Hodgson VR, Wade RP &
573 Hardeman EC. (1998). Transcription occurs in pulses in muscle fibers.
574 *Genes Dev* **12,** 2748-2758.

575

576 Ojima K, Ichimura E, Yasukawa Y, Wakamatsu J & Nishimura T. (2015). Dynamics
577 of myosin replacement in skeletal muscle cells. *Am J Physiol Cell Physiol*
578 **309,** C669-679.

579

580 Papadopoulos S, Jurgens KD & Gros G. (2000). Protein diffusion in living skeletal
581 muscle fibers: dependence on protein size, fiber type, and contraction.
582 *Biophys J* **79,** 2084-2094.

583

584 Pavlath GK, Rich K, Webster SG & Blau HM. (1989). Localization of muscle gene
585 products in nuclear domains. *Nature* **337,** 570-573.

586

587 Pilling AD, Horiuchi D, Lively CM & Saxton WM. (2006). Kinesin-1 and Dynein are
588 the primary motors for fast transport of mitochondria in Drosophila
589 motor axons. *Mol Biol Cell* **17,** 2057-2068.

590

591 Pizon V, Gerbal F, Diaz CC & Karsenti E. (2005). Microtubule-dependent
592 transport and organization of sarcomeric myosin during skeletal muscle
593 differentiation. *EMBO J* **24,** 3781-3792.

594

595 Ralston E & Hall ZW. (1992a). Restricted distribution of mRNA produced from a
596 single nucleus in hybrid myotubes. *JCB* **119,** 1063-1068.

597

598 Ralston E & Hall ZW. (1992b). Restricted distribution of mRNA produced from a
599 single nucleus in hybrid myotubes. *J Cell Biol* **119,** 1063-1068.

Ralston E, Lu Z, Biscocho N, Soumaka E, Mavroidis M, Prats C, Lomo T, Capetanaki Y & Ploug T. (2006). Blood vessels and desmin control the positioning of nuclei in skeletal muscle fibers. *J Cell Physiol* **209,** 874-882.

Ralston E, Lu Z & Ploug T. (1999). The organization of the Golgi complex and microtubules in skeletal muscle is fiber type-dependent. *J Neurosci* **19,** 10694-10705.

Romero NB. (2010). Centronuclear myopathies: a widening concept. *Neuromuscul Disord* **20,** 223-228.

Sandve GK, Gundersen S, Rydbeck H, Glad IK, Holden L, Holden M, Liestol K, Clancy T, Drablos F, Ferkingstad E, Johansen M, Nygaard V, Tostesen E, Frigessi A & Hovig E. (2011). The differential disease regulome. *BMC genomics* **12,** 353.

Sanes JR, Johnson YR, Kotzbauer PT, Mudd J, Hanley T, Martinou JC & Merlie JP. (1991). Selective expression of an acetylcholine receptor-lacZ transgene in synaptic nuclei of adult muscle fibres. *Dev* **113,** 1181-1191.

Schott DH, Collins RN & Bretscher A. (2002). Secretory vesicle transport velocity in living cells depends on the myosin-V lever arm length. *J Cell Biol* **156,** 35-39.

Smith S, Cianci C & Grima R. (2017). Macromolecular crowding directs the motion of small molecules inside cells. *J R Soc Interface* **14**.

Soh S, Banaszak M, Kandere-Grzybowska K & Grzybowski BA. (2013). Why Cells are Microscopic: A Transport-Time Perspective. *J Phys Chem Lett* **4,** 861-865.

632 Strassburger E. (1893). Über die Wirkungssphäre der kerne und die zellgrösse.
633 *Histol Beitr* **5,** 97-124.

634

635 Utvik JK, Nja A & Gundersen K. (1999). DNA injection into single cells of intact
636 mice. *Hum Gene Ther* **10,** 291-300.

637

638 van Ekeren GJ, Sengers RC & Stadhouders AM. (1992). Changes in volume
639 densities and distribution of mitochondria in rat skeletal muscle after
640 chronic hypoxia. *Int J Exp Pathol* **73,** 51-60.

641

642 Viguie CA, Lu DX, Huang SK, Rengen H & Carlson BM. (1997). Quantitative study
643 of the effects of long-term denervation on the extensor digitorum longus
644 muscle of the rat. *Anat Rec* **248,** 346-354.

645

646 Wang Z, Cui J, Wong WM, Li X, Xue W, Lin R, Wang J, Wang P, Tanner JA, Cheah
647 KS, Wu W & Huang JD. (2013). Kif5b controls the localization of myofibril
648 components for their assembly and linkage to the myotendinous
649 junctions. *Development* **140,** 617-626.

650

651 Zhou HX, Rivas G & Minton AP. (2008). Macromolecular crowding and
652 confinement: biochemical, biophysical, and potential physiological
653 consequences. *Annu Rev Biophys* **37,** 375-397.

654

655